ISBN: 978-981-18-5852-9
WCSE 2022 Spring Event: 2022 9th International Conference on Industrial Engineering and Applications
doi: 10.18178/wcse.2022.04.055

Design of Human-Machine Collaborative Control Algorithm for Lower Limb Exoskeleton

Hao-ming Li [1], Xing-song Wang [2], Meng-qian Tian [3] and Jie Wang [4]

College of Mechanical Engineering Southeast University, NanJing, 210000, China

Robotics and Biomechanics Electronics Laboratory

Abstract. In order to improve the flexibility and coordination of the exoskeleton robot, aiming at the problems of lower limb exoskeleton's poor adaptability to the external environment and poor human-machine interaction, the human-machine interaction control technology of the lower limb exoskeleton system driven by flexible bowden cable is studied in this paper. Modeling the dynamics model of the lower limb exoskeleton system driven by double bowden cable, a neural network is used to identify the wearer's movement intentions on the basis of real-time control platform, and an adaptive impedance control strategy is designed to realize the human-machine dynamic coordination. The trajectory following of the exoskeleton is implemented by torque control, and the experiments of assisted walking at different speeds prove that the lower limb exoskeleton has good dynamic adjustment performance and can realize human-machine collaboration well. The evaluation experiment of the exoskeleton's auxiliary effect is carried out, and the EMG signals prove that the human-machine collaborative control algorithm has an auxiliary effect of 5.74%-9.73%.

Keywords: Lower limb exoskeleton; Double bowden cable; Impedance control; Human-machine collaboration

1. Introduction

With the aggravation of population aging and frequent traffic accidents, there are more and more cases of weakened and impaired motor function of patients' lower limbs. For patients with lower limb injury, in addition to drug and surgical treatment, the existing main means of rehabilitation is artificial massage, but this means requires high labor intensity and certain technical experience. Lower limb exoskeleton can provide a certain degree of rehabilitation training for patients with paralysis and lower limb walking disorders, and has the characteristics of high precision and good repeatability.

Human-machine collaborative control of exoskeleton directly affects the overall performance of the exoskeleton robot, which is an important evaluation index for the assisted and rehabilitation training of the exoskeleton [1]. At present, some institutions have carried out the research on human-machine collaborative control of exoskeleton and have achieved some achievements. Stanford University in the United States proposed an impedance control algorithm based on human motion intention recognition, which is used to predict the trajectory of human body [2]. Signal and Intelligent Systems Laboratory in France proposed an impedance reduction control method for knee exoskeleton robot [3]. In addition, for nonlinear systems, the University of Wisconsin proposed a nonlinear sliding mode torque control method [4] to control the trajectory following of the upper limb exoskeleton to help human in rehabilitation training. German Aerospace Center (DLR) proposed an admittance controller based on nonlinear control equations [5], which can control the upper limb exoskeleton to lift and manipulate unknown loads.

However, the current human-machine interaction effect of the exoskeleton robots are still not ideal, and the comfort and human-machine collaboration of the exoskeleton are insufficient. To this end, we developed a wearable lower limb exoskeleton based on the bowden cable transmission system, which has lighter weight and better wearing comfort. However, bowden cable transmission has serious nonlinear characteristics, which affects the motion control effect of the joints. This paper proposes a human-machine collaborative auxiliary control algorithm for lower limb exoskeleton based on double bowden cable transmission aiming at the exoskeleton's human-machine collaborative movement [6]. The dynamics model of the exoskeleton

robot is established, and the trajectory following of the exoskeleton robot is realized by torque control. Neural network is used to identify the intention of human movement, and the impedance control strategy is used to realize dynamic coordination between human and machine. The effectiveness of the algorithm is tested through experiments. The results show that the human-machine collaborative control algorithm improves the robustness of the lower limb exoskeleton robot on the one hand, and on the other hand improves the dynamic adjustment performance of the lower limb exoskeleton, which can better realize the human-machine collaborative control.

2. Bowden cable driven lower limb exoskeleton system

The structure of lower limb exoskeleton driven by bowden cable is shown in Figure 1. Its unilateral leg has a total of 3 degrees of freedom, including two active degrees of freedom at hip joint and knee joint and one passive degree of freedom at ankle joint. The active DOF of knee joint and hip joint is driven by double bowden cable system [7].

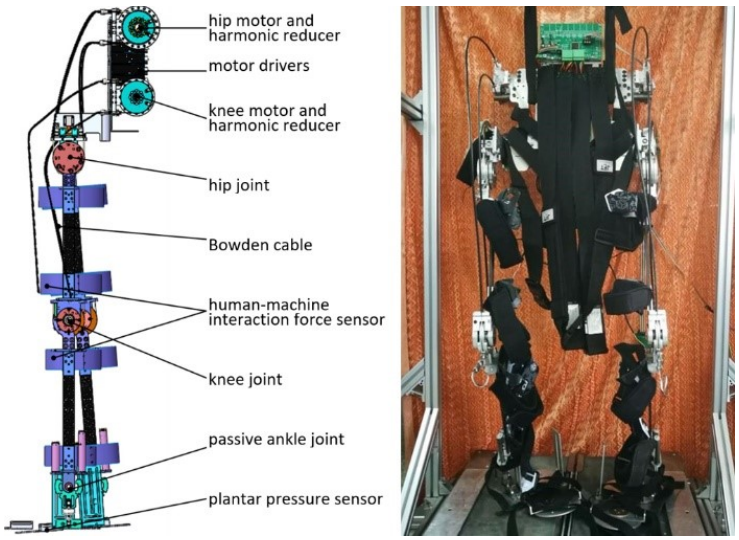

Fig. 1. Structure of exoskeleton robot

The control system of the lower limb exoskeleton robot consists of six parts: main control module, driving module, power module, data transmission module, upper computer software and sensor detection module. Among them, the main control module is composed of industrial computer's motherboard and microcontroller STM32F407. The driving module includes motor and driver. The motor is MAXON's DC servo brushed motor RE50, and the driver is ESCON70/10. The data transmission module mainly includes WIFI module, WIFI to USRT module and SD card. The WIFI module is used to transmit the sensor signal to the main control board and the upper computer software; the WIFI to USRT module mainly converts the sensor signal to the USRT signal and displays it on the upper computer interface; the SD card is mainly used to store the movement data of the exoskeleton robot, facilitate subsequent analysis and processing of data. The human-machine interaction interface of the host computer is designed based on C#, and is mainly composed of communication module, parameter adjustment module, and data display and storage module. The sensor detection module mainly includes various sensors that collect the movement data of the exoskeleton robot: the plantar pressure sensor is used to collect the pressure of the wearer's sole; the orthogonal encoder is used to collect the joint angle of the exoskeleton's joint; the human-machine interaction force sensor can measure the collaborative relationship between the human body and the exoskeleton robot, which is an important indicator of the flexibility of the control system; the EMG signal sensor collects the wearer's EMG signal, which is used to evaluate the auxiliary effect of the exoskeleton robot.

The lower limb exoskeleton robot comprehensively uses technologies such as information fusion, motion control, and intention recognition to provide protection and assistance to the wearer, thereby improving the human body's movement ability and assisting the human body's movement [8].

3. Human-machine coupling dynamics model of lower limb exoskeleton

3.1. *Double bowden cable transmission system*

The bowden cable is composed of sleeve and stainless steel wire, which can be bent at any angle in space, and its transmission path is flexible and can realize long-distance transmission. Bowden cable is widely used in multi-degree-of-freedom robots, which can effectively simplify the joint structure and greatly reduce the weight of the mechanism. There are also many cases of applying bowden cable to exoskeletons, such as the hand exoskeleton, the wearable exoskeleton and the upper limb exoskeleton [9].

The driving torque, driving displacement and transmission accuracy are mainly affected by the transmission gap and tension force during the process of bowden cable transmission [10]. The exoskeleton studied in this paper uses a double bowden cable transmission system, and its transmission model is shown in Figure 2.

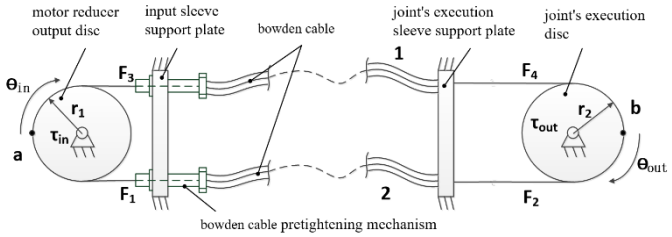

Fig. 2. Transmission model of double bowden cable

Bowden cable 1 and bowden cable 2 are installed at the joint's output disc a and the execution disc b respectively, and the pretightening force can be adjusted. F_1 and F_2 are the tension forces of bowden cable 1, F_3 and F_4 are the tension forces of bowden cable 2. θ_{in} is the rotation angle of the motor's output disc, θ_{out} is the rotation angle of the joint's execution disc, r_1 is the radius of the motor's output disc, r_2 is the radius of the joint's execution disc, τ_{in} is the input torque of the bowden cable disc, and τ_{out} is the output torque of the bowden cable. The two torques are defined clockwise as the positive direction.

It is assumed that the curvature change of the bowden cable is the same during the transmission process of the double bowden cable. Suppose the length of the bowden cable is L. At time t, the curvature of the bowden cable is $\kappa(\sigma, t)$, then the to`tal curvature of the bowden cable can be expressed as $\delta = \int_0^L \kappa(\sigma, t)\,\mathrm{d}_\sigma$, set the average curvature as k, it can be simplified to δ=kL. At this time, the tensions at the ends of bowden cable 1 and bowden cable 2 meet the following relationship:

$$F_2(t) = F_1(t)\mathrm{e}^{-\mu\kappa L} \tag{1}$$

$$F_4(t) = F_3(t)\mathrm{e}^{\mu\kappa L} \tag{2}$$

Among them, μ represents the friction coefficient between the sleeve and the steel wire.

Ignoring the rotational inertia of the small-mass bowden cable in the transmission process, the relationship between the input torque τ_{in} and the output torque τ_{out} and the bowden cable's tension can be obtained:

$$\tau_{\text{in}} = (F_1 - F_3)r_1 \tag{3}$$

$$\tau_{\text{out}} = (F_2 - F_4)r_2 \tag{4}$$

Set the internal cross-sectional of the bowden cable a and bowden cable b is A, the initial pretightening force is F_0, the elastic modulus is E, the elongation of bowden cable 1 and bowden cable 2 are ΔL_1 and ΔL_2, respectively, then the relationship is as follows:

$$\begin{aligned}\Delta L_1 &= r_1\theta_{\text{in}}(t) - r_2\theta_{\text{out}}(t) \\ &= \frac{1}{EA}\int_0^L [F_1(t)\mathrm{e}^{-\mu\kappa s} - F_0]\,\mathrm{d}s\end{aligned} \tag{5}$$

$$\begin{aligned}\Delta L_2 &= r_2\theta_{\text{out}}(t) - r_1\theta_{\text{in}}(t) \\ &= \frac{1}{EA}\int_0^L [F_3(t)\mathrm{e}^{\mu\kappa s} - F_0]\,\mathrm{d}s\end{aligned} \tag{6}$$

After integrating and simplifying the above formula, the tension of the bowden cable a and bowden cable b can be obtained to satisfy the relationship:

$$F_1 = \frac{F_3\psi_r + 2F_0L}{\psi_p} \tag{7}$$

Among them, $\psi_p = \frac{1}{\mu} - \frac{1}{\mu}e^{-\mu\kappa L}$, $\psi_r = \frac{1}{\mu} - \frac{1}{\mu}e^{\mu\kappa L}$.

Substituting equation (4) to obtain the relationship between the input torque τ_{in} and the output torque τ_{out} of driving the bowden cable disc to rotate clockwise:

$$\tau_{\text{out}} = \frac{\tau_{\text{in}} r_2}{r_1} - 2F_0 r_2 \mu\theta \tag{8}$$

In the same way, the relationship between the input torque τ_{in} and the output torque τ_{out} when rotating counterclockwise can be obtained. The transmission torque model of the double bowden cable is sorted out as follows:

$$\tau_{\text{out}}(t) = \begin{cases} \frac{\tau_{\text{in}}(t)}{n_1} - sgn(\dot{\theta}_{\text{in}})2F_0 r_2 \mu\sigma & \dot{\theta}_{\text{in}} \neq 0 \\ \tau_{\text{out}}(t^-) & \dot{\theta}_{\text{in}} = 0 \end{cases} \tag{9}$$

Among them, n_1 represents the transmission ratio, and $\text{sgn}(\dot{\theta}_{\text{in}})$ is the angular velocity switching function.

It can be seen from the above formula that the transmission performance of the double bowden cable during the working process is affected by the radius of the motor's output disc, the radius of the joint's execution disc, the initial pretightening force, the internal friction coefficient of the bowden cable and the full curvature of the bowden cable. When the speed of the double bowden cable is 0, the input torque and output torque of the transmission system are in balance; when $\tau_{\text{in}} r_2/r_1 > 2F_0 r_2 \mu\sigma$, the balance state of the double bowden cable will be destroyed. The double bowden cable transmission system enters the working state; when $\tau_{\text{in}} r_2/r_1 \leq 2F_0 r_2 \mu\sigma$, the bowden cable will enter a static state.

3.2. *Human-machine coupling dynamics modeling*

The walking process of the exoskeleton system can be divided into two stages: the single-leg support stage and the double-leg support stage. When modeling the dynamics of the exoskeleton, the exoskeleton can be simplified into a five-link model, as shown in Figure 3.

The Lagrangian method is used to model the dynamics of the exoskeleton robot, and the Lagrangian function *L* of the exoskeleton robot is defined as:

$$L = K - P \tag{10}$$

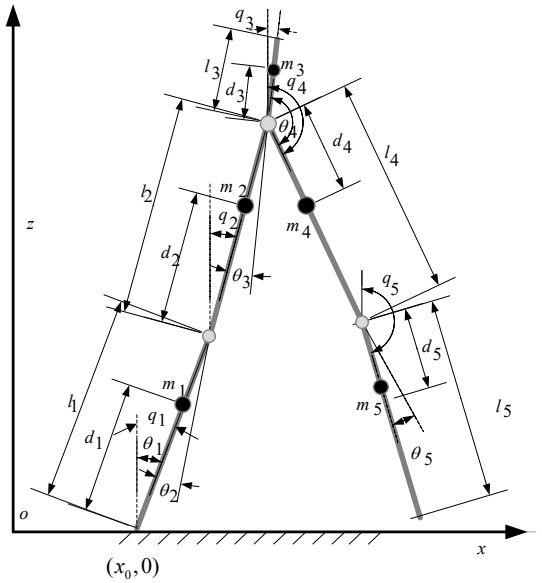

Fig. 3. Single-leg support stage schematic

Among them, *K* represents the kinetic energy of the exoskeleton robot, and *P* represents the potential energy of the exoskeleton robot.

When the exoskeleton is standing on one leg, m_i, l_i, d_i, q_i, θ_i respectively represent the mass, length, distance from the end point to the center of mass, the angle with the Z axis and the angle with previous link of the i-th link.

Establish the XOZ Cartesian coordinate system in the above model. The landing coordinates of the exoskeleton system are defined as $(x_0, 0)$. The potential energy of the system can be obtained according to the Z axis:

$$P = \sum_{i=1}^{5}(m_i g z_{c1}) \tag{11}$$

The speed of the centroid of each link on the X-axis and Z-axis can be expressed as:

$$v_c = \begin{pmatrix} \dot{x}_c \\ \dot{z}_c \end{pmatrix} \tag{12}$$

Further obtain the kinetic energy of the exoskeleton system in the single-leg support stage:

$$K = \sum_{i=1}^{5}\left(\frac{1}{2}m_i {v_{ci}}^2 + \frac{1}{2}I_i {\dot{q}_i}^2\right) \tag{13}$$

After converting the generalized coordinate q_i in the Lagrangian equation to the joint angle θ_i, substituting the kinetic energy K and the potential energy P into the equation, the Lagrangian dynamic equation can be expressed as:

$$\tau = M(\theta)\ddot{\theta} + C\left(\theta, \dot{\theta}\right) + G(\theta) \tag{14}$$

Among them, $\theta, \dot{\theta}, \ddot{\theta}$ are the angle, angular velocity and angular acceleration vector of each joint of the exoskeleton, $M(\theta)$ is a 5x5 order positive definite inertia matrix, and $C(\theta, \dot{\theta})$ is a 5x1 order Coriolis Force vector matrix, $G(\theta)$ is a 5x1 order gravity vector matrix, τ is a 5x1 order joint moment vector matrix, and the physical parameters can be obtained by measuring the exoskeleton robot.

During the double-leg support stage, the two legs share the weight of the exoskeleton system. At this time, the exoskeleton robot can be divided into two parts, left leg and right leg, and the left leg and right leg can be regarded as a three-link mechanism connected at the same end when the exoskeleton system is modeled. Similar to the process of the single-leg support stage, the coordinates of the center of mass of each link are obtained, and the derivation is performed to obtain the speed of the center of mass of each link.

The total kinetic energy K of the left leg can be expressed as:

$$K = \sum_{i=1}^{2}\left(\frac{1}{2}I_i {\dot{q}_i}^2 + \frac{1}{2}m_i {v_{ci}}^2\right) + \left(\frac{1}{2}I_{3L}{\dot{q}_3}^2 + \frac{1}{2}m_{3L}{\dot{q}_3}^2\right) \tag{15}$$

The expression of the total potential energy P of each link of the left leg is:

$$P = \sum_{i=1}^{2}(m_i g z_i) + m_{3L} g z_3 \tag{16}$$

After reorganizing and simplifying, the dynamic equation of the left leg's three-link model can be obtained as:

$$\tau_L = M_L(\theta_L)\ddot{\theta}_L + C_L\left(\theta_L, \dot{\theta}_L\right) + G_L(\theta_L) \tag{17}$$

In the same way, the dynamic equation of the right leg's three-link model can be obtained.

In the actual motion control process of the lower limb exoskeleton, there is always interaction with the human body, which is a typical human-machine coupling system. Therefore, a human-machine coupling dynamic model of the lower limb exoskeleton needs to be established for subsequent motion control.

Considering the human-machine interaction force, the exoskeleton's human-machine coupling torque model can be obtained as follows:

$$\tau_{\text{out}}\left(\theta, \dot{\theta}, \ddot{\theta}\right) = \tau\left(\theta, \dot{\theta}, \ddot{\theta}\right) + \tau_f\left(\theta, \dot{\theta}\right) + \tau_{hr} \tag{18}$$

Among them, $\tau_{\text{out}}\left(\theta, \dot{\theta}, \ddot{\theta}\right)$ represents the actual output torque of the exoskeleton's joint, $\tau\left(\theta, \dot{\theta}, \ddot{\theta}\right)$ represents the theoretical torque of the exoskeleton's joint, and $\tau_f\left(\theta, \dot{\theta}\right)$ represents the friction torque generated by the internal impedance during exoskeleton's transmission process, τ_{hr} is the human-machine interaction torque, which can be solved by the inverse kinematics of the exoskeleton and the interactive force sensor:

$$\tau_{hr} = J^T F \tag{19}$$

Among them, J^T represents the transposition of the Jacobian matrix of the contact point between the interactive force sensor and the human body.

Combined with the double bowden cable transmission model, the theoretical torque τ_{in} that the motor needs to provide can be obtained as:

$$\tau_{\text{in}}=n_1(\tau_{\text{out}}+sgn(\dot{\theta}_{\text{in}})2F_0r_2\mu\sigma)=n_1(\tau_{\text{out}}+\tau_f) \tag{20}$$

4. Design of human-machine collaborative control algorithm

In order to effectively control the flexibility of the movement between the exoskeleton robot and the human body, real-time control of the human-machine interaction force is required. This paper adopts the strategy of sub-phase control. When the movement phase of the exoskeleton system is in the swing phase, the adaptive impedance control strategy is adopted. When the movement phase is in the support phase, the static balance model is used for control. Therefore, the human-machine collaborative control algorithm needs to adapt to the change of the human body's gait phase, and judge the human body's movement intention in real time, then perform assist control in accordance with the human body's movement intention.

4.1. *Human intention recognition*

The recognition of human movement intention mainly includes the recognition of gait phase and movement trend. The gait cycle of the human body and the landing state of the feet have a corresponding relationship. The identification of the phase of the human body's movement gait can be realized by judging the state of the soles of the two feet. In this paper, a corresponding plantar pressure sensor is designed to measure the plantar pressure of the human body during walking in real time. The plantar pressure is a great indicator of whether the feet are in contact with the ground during walking. Therefore, it is only necessary to set a certain threshold for the plantar pressure signal of the human body to achieve better recognition of support phase and swing phase in human gait.

On the basis of recognizing the support phase and swing phase of the human body, it is necessary to further determine the movement trend is flexion or extension, so as to realize the dynamic collaborative response between the exoskeleton system and the human body. To this end, we propose a neural network algorithm based on plantar pressure and joint angle to identify the human body's movement intention. The plantar pressure and joint angle are used as the criterion to identify the movement intention of the human body. Using the radial basis neural network algorithm to learn the human body's motion intention offline, selecting the exoskeleton robot's angle sensor and plantar pressure sensor as the input of the neural network, and using the RBF neural network to judge the human body's motion intention.

Among them, the input layer variables include $\mathrm{x}_1(\mathrm{t})$ and $\mathrm{x}_2(\mathrm{t})$, the $\mathrm{x}_1(\mathrm{t})$ vector includes the orthogonal encoder angles at the left/right hip and left/right knee joints at time t, and the $x_2(t)$ vector includes the pressure of the left heel/foot and the pressure of the right heel/foot at time t; the output layer variable H(t) represents the gait phase of the exoskeleton robot.

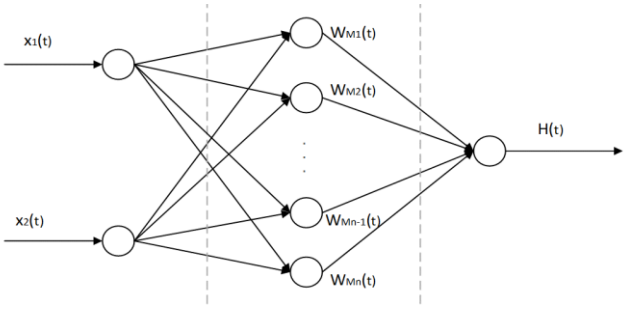

Fig. 4. Schematic diagram of RBF neural network

In the RBF neural network structure, the input variable is expressed as X=[x_1,x_2, ⋯,x_n], which is mapped to the hidden layer with Gaussian radial basis function:

$$H_j=exp\left(-\frac{\left||X-c_j|\right|^2}{2{\sigma_j}^2}\right),j=1,2,\cdots,n \tag{21}$$

Among them, H_j represents the output of the node's hidden layer, c_j represents the center vector of the jth node, σ_j represents the base width of the jth node, and n represents the number of hidden nodes.

In order to simplify the structure, a neural network structure with one hidden layer is selected, and the number of neurons in the hidden layer is 10. The sample data is divided into training data, verification data, and test data. The proportion of the sample data is 70% as the training data, 15% as the verification data, and 15% as the test data. After training, there is no under-fitting and over-fitting. The linear regression values of the training results, verification results and test results are 0.9789, 0.9226, 0.90828 respectively, and the final R value of the total training output 0.96404, which meets the needs of the exoskeleton system for phase judgment.

4.2. *Design of Impedance controller*

Since the impedance control strategy is applicable to the swing phase of the exoskeleton, combined with the RBF neural network introduced in the previous section to determine the movement phase of the exoskeleton robot. If the exoskeleton robot is in the support phase, the static balance model is selected for control; if the exoskeleton robot is in the swing phase, the impedance controller is selected for motion control, and the control strategy is shown in Figure 4.

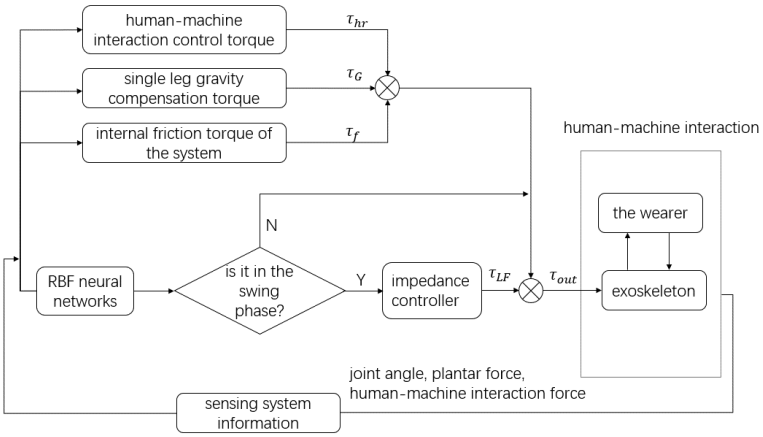

Fig. 5. Impedance controller's block diagram

The impedance control algorithm can be expressed as:

$$M_d(t)\big(\ddot{\theta}(t)\big) + C_d(t)\big(\dot{\theta}(t)\big) + G_d(t)(\theta(t)) = f(t) \tag{22}$$

Among them, $M_d(t)$ represents the ideal inertial matrix in the impedance control model, $C_d(t)$ represents the ideal damping matrix in the impedance control model, $G_d(t)$ represents the ideal stiffness matrix in the impedance control model, $\theta(t)$ represents the joint angle of the exoskeletal system, and $f(t)$ represents the human-machine interaction force.

The angular velocity and angular acceleration are obtained by directly deriving the joint angle obtained by the encoder, which will magnify the error. In order to avoid the influence of excessive error, we change the dynamic equation of the exoskeleton system to obtain the joint acceleration vector. Expressed as:

$$\begin{aligned}\ddot{\theta} = (M(\theta))^{-1}(n_1 \cdot \tau_{\text{in}} - C\big(\theta, \dot{\theta}\big) \\ -G(\theta) - \tau_f\big(\theta, \dot{\theta}\big) - \tau_{hr})\end{aligned} \tag{23}$$

After further sorting, the available control law is as follows:

$$\begin{aligned}u = M_d(\theta)(\ddot{\theta}(t)\big) - f(t) + C_d(t)\left(\dot{\theta}(t)\right) \\ +G_d(t)\big(\theta(t)\big) + C\big(\theta, \dot{\theta}\big) \\ +G(\theta) + \tau_f\big(\theta, \dot{\theta}\big) + \tau_{hr}\end{aligned} \tag{24}$$

It can be seen from the above design process that if the parameters of the impedance controller are all fixed, it is difficult for the controller to change with the external environment, and thus cannot adapt to the real-time interaction between the exoskeleton system and the external environment. Therefore, the inertial matrix $M_d(t)$ of the impedance controller designed in this paper is selected as the actual inertial matrix of the

exoskeleton system, and the damping parameter $C_d(t)$ and the stiffness parameter $G_d(t)$ are set as adjustable parameters for real-time online renew.

When adjusting the parameters of the impedance controller, the target penalty function of the impedance controller needs to include the interaction force between human and machine, and the magnitude of its human-machine interaction force will vary according to the output of the RBF neural network, which is specifically defined as :

$$\Gamma(t) = \int_0^{ts} f(t)^T Q f(t) \mathrm{d}t \tag{25}$$

In the control law of equation (34), only the damping parameter $C_d(t)$ and the stiffness parameter $G_d(t)$ need to be calculated in real time, that is, to realize the online adjustment of the impedance control's parameters. In this paper, the steepest gradient descent method is used to adjust the parameters of impedance control online, and iterative optimization is continuously carried out by using the negative gradient direction of the parameters as the target direction.

The update process of design damping parameter $C_d(t)$ and stiffness parameter $G_d(t)$ is shown in the following formula:

$$C_d^k(t) = C_d^{k-1}(t) - \beta_c \left(\frac{\partial \Gamma^k(t)}{\partial C_d^k(t)}\right)^T \tag{26}$$

$$G_d^k(t) = G_d^{k-1}(t) - \beta_G \left(\frac{\partial \Gamma^k(t)}{\partial G_d^k(t)}\right)^T \tag{27}$$

Among them, β_c represents the learning rate of the damping parameter updating; β_G represents the learning rate of the stiffness parameter updating, and satisfies $\beta_G < 1$; $C_d^k(t)$, $C_d^{k-1}(t)$ respectively represent the damping parameter and damping parameter at time k; $G_d^k(t)$, $G_d^{k-1}(t)$ respectively represent the stiffness parameter at time k and the stiffness parameter at time k-1.

At this point, the control law of the exoskeleton system can be obtained as:

$$\begin{aligned} u^k = M(\theta_k(t))\left(\ddot{\theta}^k(t)\right) - f_k(t) + C_d^k(t)\left(\dot{\theta}_k(t)\right) \\ + G_d^k(t)\left(\theta_k(t)\right) + C\left(\theta_k(t), \dot{\theta}_k(t)\right) + G\left(\theta_k(t)\right) \\ + \tau_f\left(\theta_k(t), \dot{\theta}_k(t)\right) + \tau_{hr}^k \end{aligned} \tag{28}$$

The control law can be obtained in real time. Among them, $M(\theta_k(t))$, $C\left(\theta_k(t), \dot{\theta}_k(t)\right)$, $G(\theta_k(t))$ can be obtained by calculating the position feedback and speed feedback of the encoder conbined with human-machine coupling dynamics model. $C_d^k(t)$, $G_d^k(t)$ can be updated in real time by the above-mentioned steepest descent method; $\theta_k(t)$, $\dot{\theta}_k(t)$ respectively represent the actual joint angle and actual joint angular velocity. Based on the exoskeleton system's dynamics model and the human-machine coupling interaction model, combined with the information of the orthogonal encoder and the human-machine interaction force sensor, the adaptive impedance control law of the exoskeleton system can be obtained.

4.3. *Experiments and analysis*

During the experiment, when the gait cycle of the exoskeleton robot is in the support phase, the static balance model is used for control, and the human-machine interaction force is not controlled; when the gait cycle of the exoskeleton robot is in the flexion phase, the ideal value of the human-machine interaction force is set to 20N; when the gait cycle of the exoskeleton robot is in the extension phase, the ideal value of the human-machine interaction force is set to -20N; this paper uses an industrial computer for experimental verification, using Simulink's block diagram to realize the design of impedance controller. As shown in Figure 6, the experimenter wears the exoskeleton robot to perform assisted walking experiments on a treadmill at different paces. The experimental results are shown in Figure 7.

Fig. 6. Lower limb exoskeleton walking test

From the experimental results, when the human body is walking slowly at a speed of 2km/h, the control system can well recognize the human body's movement intention and assist it, and the force on the human body is stably maintained at 20N; when the human body is walking at 5km/h, the human body's flexion and extension change quickly because of the gait cycle is shortened, and the force of the controller on the human body fluctuates greatly, and it appears peak during the transition between flexion and extension. On the whole, it can still recognize the human body's movement intention, and assist in the control of the human body's movement intention. Therefore, the impedance controller designed in this paper can control the exoskeleton system to assist the human body when walking at different speeds, achieving a better human-machine interaction effect, and the lower the speed, the better the control effect, and the human-machine interaction is more stable.

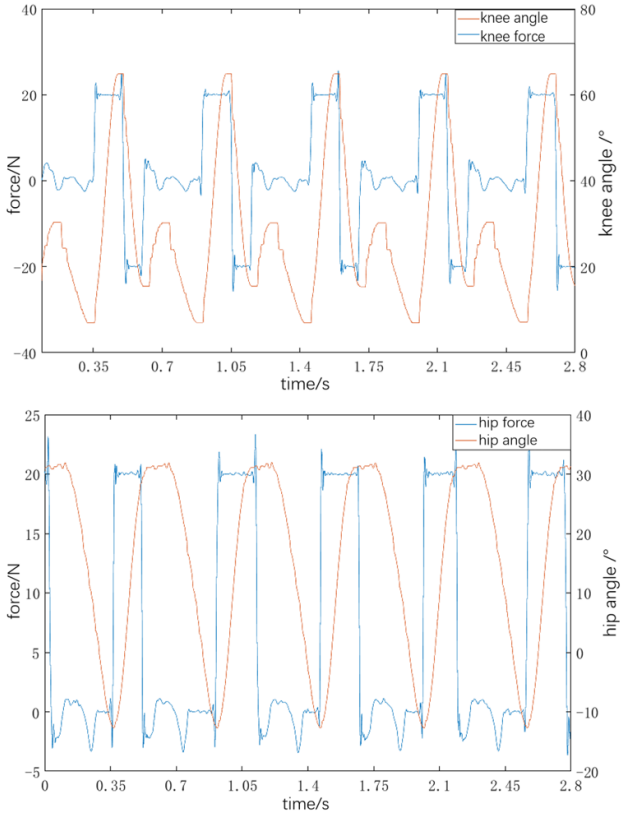

(a) Exoskeleton walking curve at 2km/h

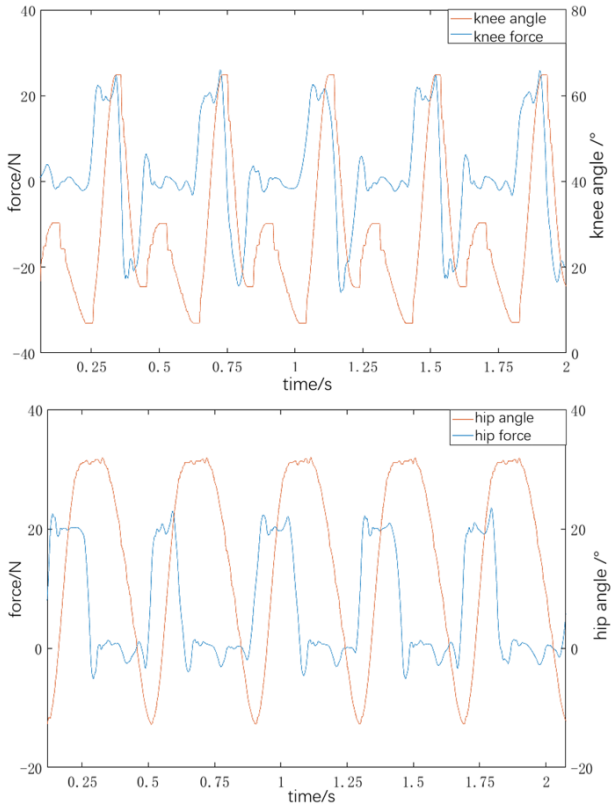

(b) Exoskeleton walking curve at 5km/h

Fig. 7. Exoskeleton walking assist curve

In order to evaluate the assisted effect of the exoskeleton's human-machine collaborative control system, this paper carried out two comparative experiments on the treadmill experimental platform for normal walking and walking with exoskeleton's assistant. The surface EMG signals of the rectus femoris and biceps femoris muscles are collected, as shown in Figure 8. It can be seen that when the human body wears the exoskeleton for assisted control, the amplitude of the EMG signal value of its rectus femoris and biceps femoris muscles has a certain decrease, indicating that the muscle activation is low and the muscles are more relaxed.

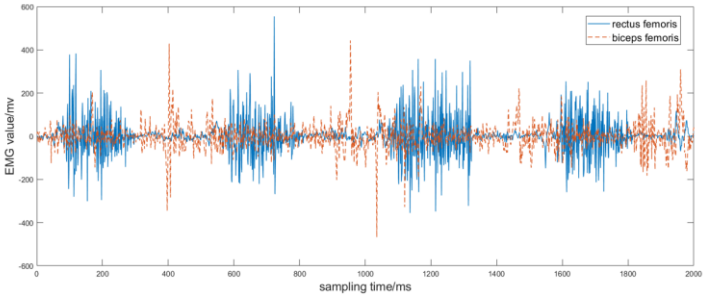

(a) Natural motion of human body

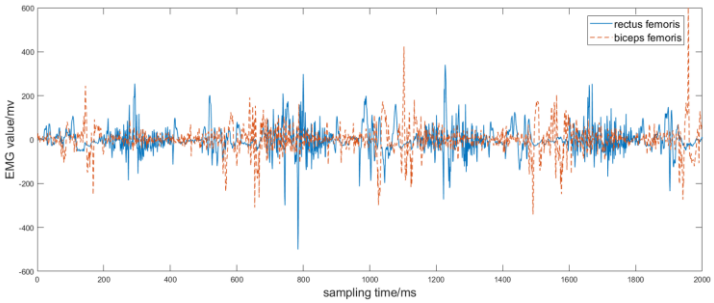

(b) Exoskeleton assist status

Fig. 8. Original curve of EMG signal

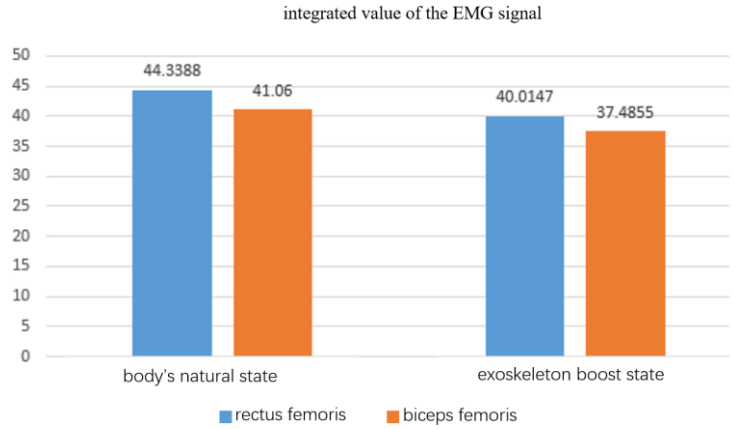

Fig. 9. Integral of EMG signal

Studies have shown that the magnitude of the integrated value of the EMG signal is positively correlated with the degree of muscle activity, the EMG signal is integrated, and the result is shown in Figure 9. It can be seen that the integrated EMG value of wearing exoskeleton is reduced by 9.75% and 8.71% respectively compared with the EMG signal value in the natural state. The results show that: the wearer's muscle activity is reduced, and his muscle's power output is reduced, indicating that the exoskeleton has a certain boosting effect.

5. Conclusion

In this paper, through the research and analysis of the lower limb exoskeleton system of the double bowden cable transmission, and the analysis and modeling of the double bowden cable transmission, combined with the dynamic model of the lower limb exoskeleton, a human-machine coupling dynamics model is built. The static balance model is used for control in the support phase, and the impedance control algorithm is used in the swing phase. The target penalty function is set according to the human-machine interaction force, using the steepest descent method to continuously adjust the impedance controller's parameters, and set the exoskeleton robot different walking speeds to control, verifying that the designed impedance controller can achieve good human-machine collaborative control effect. And through experiments to evaluate the boosting effect of the exoskeleton system, it is proved that the exoskeleton robot can reach a boosting effect of 5.47%-9.75%.

6. References

[1] Y. WANG, A. ZHU, H. WU, P. ZHU, X. ZHANG and G. CAO, "Control of lower limb rehabilitation exoskeleton robot based on CPG neural network*," 2019 16th International Conference on Ubiquitous Robots (UR), 2019, pp. 678-682, doi: 10.1109/URAI.2019.8768691.

[2] B. Hu, H. Yu, H. Lu and Y. Chang, "Design of mechanism and control system for a lightweight lower limb exoskeleton," 2018 3rd International Conference on Control, Robotics and Cybernetics (CRC), 2018, pp. 83-87, doi: 10.1109/CRC.2018.00025.

[3] M. Gilbert, X. Zhang and G. Yin, "Modeling and design on control system of lower limb rehabilitation exoskeleton robot," 2016 13th International Conference on Ubiquitous Robots and Ambient Intelligence (URAI), 2016, pp. 348-352, doi: 10.1109/URAI.2016.7734058.

[4] P. Chen, "Key analysis of research progress on lower limb exoskeleton robots," 2021 International Conference on Artificial Intelligence and Electromechanical Automation (AIEA), 2021, pp. 78-83, doi: 10.1109/AIEA53260.2021.00024.

[5] Y. M. Pirjade, D. R. Londhe, N. M. Patwardhan, A. U. Kotkar, T. P. Shelke and S. S. Ohol, "Design and fabrication of a low-cost human body lower limb exoskeleton," 2020 6th International Conference on Mechatronics and Robotics Engineering (ICMRE), 2020, pp. 32-37, doi: 10.1109/ICMRE49073.2020.9065128.

[6] Y. Wu, G. -Z. Cao, S. -D. Huang and Y. Peng, "Distributed database of cloud platform for the lower-limb

exoskeleton robot," 2020 17th International Conference on Ubiquitous Robots (UR), 2020, pp. 322-326, doi: 10.1109/UR49135.2020.9144697.

[7] Y. Wang, Z. Liu, L. Zhu, X. Li and H. Wang, "An impedance control method of lower limb exoskeleton rehabilitation robot based on predicted forward dynamics," 2020 IEEE 19th International Conference on Trust, Security and Privacy in Computing and Communications (TrustCom), 2020, pp. 1515-1518, doi: 10.1109/TrustCom50675.2020.00206.

[8] G. E. Dongming, S. Guanghui, Z. Yuanjie and S. Jixin, "Impedance control of multi-arm space robot for the capture of non-cooperative targets," in Journal of Systems Engineering and Electronics, vol. 31, no. 5, pp. 1051-1061, Oct. 2020, doi: 10.23919/JSEE.2020.000079.

[9] Phan Thanh Phuc, Nguyen Dao Xuan Hai, and Nguyen Truong Thinh, "Design adaptive fuzzy sliding mode controller for pantograph mechanism apply to massage therapy robot for healthcare," Journal of Automation and Control Engineering, Vol. 7, No. 1, pp. 13-23, June, 2019. doi: 10.18178/joace.7.1.13-23.

[10] C. K. Huang, C. Y. Yang, B. C. Hsu, Yi-Ying Lin, and C. H. Chen, "An automatic 3D work object calibration method based on hybrid 2D image vision," Journal of Automation and Control Engineering, Vol. 8, No. 1, pp. 20-25, June, 2020. doi: 10.18178/joace.8.1.20-25.